Employing three-blade propeller lanthanide complexes as molecular luminescent thermometers: study of temperature sensing through a concerted experimental/theory approach

Dmitry Lyubov, Albano Carneiro Neto, Ahmad Fayoumi, Konstantin Lyssenko, Vladislav Korshunov, Ilya Taydakov, Fabrice Salles, Yannick Guari, Joulia Larionova, Luis Carlos, et al.

Employing three-blade propeller lanthanide complexes as molecular luminescent thermometers: study of the temperature sensing through a concerted experimental/theory approach

Dmitry M. Lyubov,[a,b] Albano N. Carneiro Neto,*[c] Ahmad Fayoumi,[a] Konstantin A. Lyssenko,[b,d] Vladislav M. Korshunov,[e] Ilya V. Taydakov,[b,e] Fabrice Salles,[f] Yannick Guari,[f] Joulia Larionova,[f] Luis D. Carlos,[c] Jérôme Long,*[f,g] Alexander A. Trifonov*[a,b]

[a.] *Institute of Organometallic Chemistry of Russian Academy of Sciences, 49 Tropinina str., GSP-445, 630950, Nizhny Novgorod, Russia. E-mail: trif@iomc.ras.ru*
[b.] *Institute of Organoelement Compounds of Russian Academy of Sciences, 28 Vavilova str., 119334 , Moscow, Russia.*
[c.] *Department of Physics and CICECO – Aveiro Institute of Materials, University of Aveiro, 3810-193, Aveiro, Portugal. Email: albanoneto@ua.pt*
[d.] *Lomonosov Moscow State Univ, Dept. Chem, Leninskie Gory 1, Build 3, Moscow 119991, Russia.*
[e.] *P. N. Lebedev Physical Institute of the Russian Academy of Sciences, Leninskiy Prospect 53, 119991, Moscow, Russia*
[f.] *ICGM, Univ. Montpellier, CNRS, ENSCM, Montpellier, France. E-mail : jerome.long@umontpellier.fr*
[g.] *Institut Universitaire de France (IUF), 1 rue Descartes, 75231 Paris Cedex 05, France*

We report the synthesis, structures, magnetic and luminescent properties of a series of three-blade propeller homoleptic lanthanide complexes $[LnL_3](ClO_4)_3 \cdot H_2O \cdot 2MeCN$ (Ln = Eu (**1**), Tb (**2**), Dy (**3**), Er (**4**), Yb (**5**), Gd (**6**); L = 2,6-bis(1-methyl-imidazol-2-yl)pyridine). The Eu, Tb, and Dy analogues exhibit the characteristic lanthanide-based luminescence. Remarkably, the mixed Eu/Tb complex with a metal ratio (1:10) can be used as a ratiometric thermometer in the solid-state between 130–220 K with the maximum value of S_r = 6.6 %·K^{-1} within the range of 150–170 K. Theoretical calculations allow not only to model the luminescence properties of pure complexes but also rationalize the performances of the mixed Eu/Tb thermometers.

Introduction

Coordination complexes based on lanthanide ions have recently emerged as promising candidates for the design of molecule-based devices owing to both their exceptional optical and magnetic features.[1] On one hand, these molecular complexes could retain their magnetization when an appropriate alliance between the 4*f* electronic density and a specific coordination environment is chemically engineered.[2-7] On the other hand, the usual spin and parity forbidden *f-f* electronic transitions might give rise to exceptional luminescence features in Ln^{3+}-based materials, characterized by long-lived emission, narrow bandwidth, large Stokes shifts (or ligand-induced Stokes shifts, excitation in the UV within ligands states and luminescence in visible/near-infra red spectral range due to 4*f*-4*f* transitions), and generally high luminescence quantum yields.[8-12]

Although direct light excitation in the 4*f* levels could be employed to generate luminescence, the so-called “antenna effect” is usually preferred to provide highly-luminescent systems.[13] This approach relies on a light-induced energy transfer between the excited states related to both the surrounding ligand and the Ln^{3+} ion. This latter afterwards emits its characteristic luminescence. Such a process however requires an optimal energy match and selection rules between the different excited levels for an efficient energy transfer.[14] Moreover, minimizing deactivation processes related to O–H vibrations and coordinated solvent molecules appears also critical.[13] This could be achieved by tailoring a rigid lanthanide environment in which the Ln^{3+} ion is sheltered from solvent interactions.[15]

Taking into account the rich versatility in the coordination number/environment of lanthanide ions, designing 4*f* complexes with rigid scaffolds has been widely performed using open-chain or macrocyclic ligands. In particular, the D_3-symmetry complexes such as for instance $[Ln(dipic)]^{3-}$ (dipic = pyridyl-2,6-dicarboxylate), represent interesting examples owing to their emissive performances.[16] The D_3 symmetry arrangement of the three ligands around the lanthanide ion engenders chiral complexes that exist as a racemic mixture in solution or solid-state in standard conditions. Such feature could be taken as an advantage to sense the chirality of optically active molecules (sugars or amino-acids).[17-20]

Despite the fact that lanthanide emission features are extremely sensitive to the ligand backbone, the number of D_3 lanthanide complexes based on purely nitrogen ligands is relatively limited.[21-30] For instance, a few examples of transition metal complexes based on the tridentate 2,6-bis(1-methyl-imidazol-2-yl)pyridine (L) ligand have been reported.[31-32] Up to now, its use towards lanthanide ions has not been addressed to the best of our knowledge.

In this regard, one of the recent development of lanthanide luminescence concerns the possibility to sense the temperature using the emission features.[33] This non-invasive spectroscopic method benefits from a high relative thermal sensitivity (S_r > 1 %·K^{-1}), spatial resolution (< 10 μm) in short acquisition times (< 1 ms) and has become popular in the last decade due to its enormous potential[34-35] as the conventional thermometers reach their limits. One of the most straightforward strategy to leverage the luminescence for thermal sensing consists in monitoring the luminescence intensity ratio (LIR) of two electronic transitions in thermal equilibrium.[34, 36-40] This LIR-based thermometry allows to overcome some constraints affecting the performance of luminescent thermometers based on an unique emission band.[34, 36-37] The LIR approach encompasses both, single-ion[41-43] and dual-center-examples,[44-50] for which the latter are widely based on solid-solution materials based on the Eu^{3+}/Tb^{3+} pair. Such interest could be explained by the exceptional luminescence features of both Eu^{3+}/Tb^{3+} ions which could be carefully optimized by varying the nature of the sensitizer ligand. Moreover, these Eu^{3+}/Tb^{3} systems show greater quantum yield which is relevant for thermometry applications. In comparison to Ln^{3+}-based inorganic phosphors, [34, 51-54] molecule-based materials present several assets: *i*) they are usually obtained using soft chemistry routes; *ii*) they benefit from a light density and optical transparency; *iii*) they could be easily of shaped. They also offer an almost unlimited structural diversity depending on the choice of metal ion/ligand. All together, these concepts could be efficiently used to control the parameters affecting the thermometric parameters by the careful choice of the building blocks (lanthanide ion, ligands, and in turn the intermolecular distances). Yet and contrary to a common belief, the thermometric performances do not always systematically rely on a Tb^{3+}-to-Eu^{3+} energy transfer, as it strongly depends on the distance between the two centers. For instance, some of us recently demonstrated that in strictly molecular complexes with sufficient long intermolecular distances, the thermometric performances are mainly driven by the energy transfer between the singlet and triplet ligand states with the Tb^{3+} and Eu^{3+} excited states.[55]

Following this, we propose here to take advantage of the impressive luminescent properties of D_3 lanthanide complexes to design original and sensitive luminescent thermometers. We therefore report in this article the synthesis, structures, luminescent, magnetic properties of a series of robust three-blade propeller lanthanide complexes based on the tridentate nitrogen-based ligand 2,6-bis(1-methyl-imidazol-2-yl)pyridine (L). At the exception of the Er analogue, the complexes exhibit a lanthanide-based luminescence. Using a concerted experimental/theory approach, we investigate and rationalize the thermometric performances of the mixed Eu/Tb complexes.

Experimental

General Procedures

The synthesis of complexes **1–6** was performed under aerobic conditions. Acetonitrile was distilled prior to use. 2,6-Bis(1-methyl-imidazol-2-yl)pyridine (L) was prepared according to the literature procedure.[56] IR spectra were recorded as Nujol mulls on a Bruker-Vertex 70 spectrophotometer. The C, H, N elemental analyses were carried out in the microanalytical laboratory of the IOMC by means of a Carlo Erba Model 1106 elemental analyzer with an accepted tolerance of 0.4 units on carbon (C), hydrogen (H), and nitrogen (N). Lanthanide metal analysis was carried out by complexometric titration.[57]

Synthesis of $[LnL_3](ClO_4)_3·H_2O·2MeCN$. A mixture of $Eu(ClO_4)_3(H_2O)_6$ (0.170 g, 0.30 mmol) and ligand L (0.240 g, 1.00 mmol, 3.3 equiv.) was dissolved in MeCN (30 mL) at ambient temperature. The concentration of the resulting clear solution at ambient temperature gives colorless crystals of **1**. The solution was decanted and the crystals were washed with a small amount of MeCN and dried at ambient conditions overnight. Complex **1** was isolated in 86% yield (0.332 g, 0.26 mmol). Complexes $[LnL_3](ClO_4)_3·H_2O·2MeCN$ (Ln = Tb (**2**), Dy (**3**), Er (**4**), Yb (**5**), Gd (**6**)) were prepared following the similar procedure and were isolated as almost colorless crystals in 83 (for **2**), 76 (for **3**), 72 (for **4**), 65% (for **5**), and 69% (for **6**) yields respectively.

Characterization of **$[EuL_3](ClO_4)_3·H_2O·2MeCN$ (1)**: Elemental analysis calcd. (%) for $C_{43}H_{47}Cl_3EuN_{17}O_{13}$ (1268.26 g/mol): C, 40.72; H, 3.74; N, 18.77; Eu, 11.98. Found: C, 40.68; H, 3.70; N, 18.90; Eu, 12.02. IR (Nujol, KBr) ν/cm^{-1}: 485 (w), 620 (s), 655 (w), 695 (s), 705 (s), 735 (m), 770 (m), 785 (m), 810 (s), 940 (s), 995 (m), 1050 (m), 1090 (s), 1155 (s), 1190 (s), 1230 (m), 1265 (s), 1290 (s), 1350 (m), 1415 (m), 1485 (s), 1495 (s), 1545 (w), 1570 (s), 1600 (s), 1635 (w), 1715 (m), 2025 (m), 2240 (w), 3130 (s), 3540 (s).

Characterization of **$[TbL_3](ClO_4)_3·H_2O·2MeCN$ (2)**: Elemental analysis calcd. (%) for $C_{43}H_{47}Cl_3N_{17}O_{13}Tb$ (1275.22 g/mol): C, 40.50; H, 3.71; N, 18.67; Tb, 12.46. Found: C, 40.39; H, 3.82; N, 18.64; Tb, 12.53. IR (Nujol, KBr) ν/cm^{-1}: 490 (w), 625 (s), 655 (w), 695 (s), 705 (s), 735 (m), 745 (m), 770 (m), 810 (s), 945 (s), 1000 (m), 1050 (m), 1100 (s), 1160 (s), 1190 (s), 1230 (m), 1265 (s), 1290 (s), 1350 (m), 1410 (m), 1490 (s), 1545 (w), 1570 (s), 1600 (s), 1645 (w), 1735 (m), 2030 (m), 2240 (w), 3130 (s), 3145 (m), 3165 (w), 3450 (m), 3550 (m), 3620 (s).

Characterization of **$[DyL_3](ClO_4)_3·H_2O·2MeCN$ (3)**: Elemental analysis calcd. (%) for $C_{43}H_{47}Cl_3DyN_{17}O_{13}$ (1278.80 g/mol): C, 40.39; H, 3.70; N, 18.62; Dy, 12.71. Found: C, 40.21; H, 3.64; N, 18.78; Dy, 12.63. IR (Nujol, KBr) ν/cm^{-1}: 490 (w), 620 (s), 655 (w), 695 (s), 705 (s), 735 (m), 745 (m), 770 (w), 810 (s), 945 (s), 1000 (m), 1050 (m), 1100 (s), 1160 (s), 1190 (s), 1230 (m), 1265 (s), 1290 (s), 1350 (m), 1410 (m), 1490 (s), 1545 (w), 1570 (s), 1600 (s), 1645 (w), 1735 (m), 2030 (m), 2240 (w), 3125 (s), 3145 (m), 3165 (w), 3445 (m), 3550 (m), 3625 (s).

Characterization of **$[ErL_3](ClO_4)_3·H_2O·2MeCN$ (4)**: Elemental analysis calcd. (%) for $C_{43}H_{47}Cl_3ErN_{17}O_{13}$ (1283.56 g/mol): C, 40.24; H, 3.69; N, 18.55; Er, 13.03. Found: C, 40.11; H, 3.57; N, 18.46; Er, 12.94. IR (Nujol, KBr) ν/cm^{-1}: 490 (w), 620 (s), 655 (w), 695 (s), 705 (s), 735 (m), 745 (m), 775 (w), 810 (s), 945 (s), 1000 (m), 1050 (m), 1100 (s), 1160 (s), 1190 (s), 1230 (m), 1270 (s), 1290 (s),

1355 (m), 1410 (m), 1490 (s), 1540 (w), 1570 (s), 1600 (s), 1650 (w), 1730 (m), 2030 (m), 2240 (w), 3125 (s), 3145 (m), 3165 (w), 3440 (m), 3550 (m), 3620 (m).

Characterization of **[YbL$_3$](ClO$_4$)$_3$·H$_2$O·2MeCN (5)**: Elemental analysis calcd. (%) for $C_{43}H_{47}Cl_3N_{17}O_{13}Yb$ (1289.35 g/mol): C, 40.06; H, 3.67; N, 18.47; Yb, 13.42. Found: C, 39.98; H, 3.70; N, 18.38; Yb, 13.35. IR (Nujol, KBr) ν/cm^{-1}: 490 (w), 620 (s), 655 (w), 695 (s), 705 (s), 735 (m), 745 (m), 785 (w), 810 (s), 945 (s), 1000 (m), 1050 (m), 1100 (s), 1160 (s), 1190 (s), 1230 (m), 1270 (s), 1290 (s), 1355 (m), 1410 (m), 1490 (s), 1540 (w), 1570 (s), 1600 (s), 1650 (w), 1720 (m), 2025 (m), 2240 (w), 3125 (s), 3145 (m), 3165 (w), 3440 (m), 3545 (m), 3620 (m).

Characterization of **[GdL$_3$](ClO$_4$)$_3$·H$_2$O·2MeCN (6)**: Elemental analysis calcd. (%) for $C_{43}H_{47}Cl_3GdN_{17}O_{13}$ (1273.55 g/mol): C, 40.55; H, 3.72; N, 18.70; Gd, 12.35. Found: C, 40.67; H, 3.79; N, 18.54; Gd, 12.19. IR (Nujol, KBr) ν/cm^{-1}: 490 (w), 620 (s), 655 (w), 695 (s), 705 (s), 735 (m), 745 (m), 785 (w), 810 (s), 945 (s), 1000 (m), 1050 (m), 1100 (s), 1160 (s), 1190 (s), 1230 (m), 1270 (s), 1290 (s), 1355 (m), 1410 (m), 1490 (s), 1540 (w), 1570 (s), 1600 (s), 1650 (w), 1720 (m), 2025 (m), 2240 (w), 3125 (s), 3145 (m), 3165 (w), 3440 (m), 3545 (m), 3620 (m).

The mixtures of Eu/Tb complexes [Eu$_{0.09}$Tb$_{0.91}$L$_3$](ClO$_4$)$_3$·H$_2$O·2MeCN (**Eu$_{0.09}$Tb$_{0.91}$**), [Eu$_{0.50}$Tb$_{0.50}$L$_3$](ClO$_4$)$_3$·H$_2$O·2MeCN (**Eu$_{0.50}$Tb$_{0.50}$**) and [Eu$_{0.83}$Tb$_{0.17}$L$_3$](ClO$_4$)$_3$·H$_2$O·2MeCN (**Eu$_{0.83}$Tb$_{0.17}$**) were prepared by dissolution of calculated amounts of **1** and **2** (1:10, 1:1 and 5:1 molar ration respectively) in MeCN and further crystallization from the resulted solution by slow concentration at ambient temperature. Elemental analysis calcd. (%) for $C_{43}H_{47}Cl_3N_{17}O_{13}$**Eu$_{0.09}Tb_{0.91}$** (1274.59 g/mol): C, 40.52; H, 3.72; N, 18.68; Eu, 1.08; Tb, 11.34 (total Ln^{3+} 12.42). Found: C, 40.69; H, 3.80; N, 18.55; total Ln^{3+} 12.35. Elemental analysis calcd. (%) for $C_{43}H_{47}Cl_3N_{17}O_{13}$**Eu$_{0.5}Tb_{0.5}$** (1277.75 g/mol): C, 40.61; H, 3.73; N, 18.72; Eu, 5.97; Tb, 6.25 (total Ln^{3+} 12.22). Found: C, 40.38; H, 3.85; N, 18.66; total Ln^{3+}, 12.11. Elemental analysis calcd. (%) for $C_{43}H_{47}Cl_3N_{17}O_{13}$**Eu$_{0.83}Tb_{0.17}$** (1269.42 g/mol): C, 40.68; H, 3.73; N, 18.76; Eu, 9.98; Tb, 2.09 (total Ln^{3+} 12.07). Found: C, 40.77; H, 3.89; N, 18.85; total Ln^{3+} 12.01.

X-Ray crystallography

X-ray diffraction investigations were carried out on a Bruker D8 QUEST single-crystal X-ray diffractometer equipped with with Photon II charge-integrating pixel array detector (CPAD), laterally graded multilayer (Goebel) mirror and microfocus Mo-target X-ray tube (λ = 0.73071 Å). Data reduction and integration were performed with the Bruker software package SAINT. The absorption correction was performed using the multiscan routine as implemented in SADABS program.[58] All structures were solved by direct methods using SHELXS-2013/SHELXT[59] and refined against F^2 using SHELXL-2018.[60] Upon the refinement of the anisotropic displacement parameters of the disordered ClO_4^- anions the ISOR restraint for some oxygen atoms were applied. All hydrogen atoms were placed in ideal calculated positions and refined as riding atoms with relative isotropic displacement parameters. The SHELXTL program suite was used for molecular graphics. Crystal data, data collection, and structure refinement details are summarized in Table S1 of SI. CCDC numbers 2095653–2095657 for compounds **1–5** contain the supplementary crystallographic data for this paper. These data are provided free of charge by The Cambridge Crystallographic Data Centre: ccdc.cam.ac.uk/structures.

Magnetic Measurements

Magnetic susceptibility data were collected with a Quantum Design MPMS-XL SQUID magnetometer working in the range 1.8–350 K with the magnetic field up to 7 Tesla. The samples were prepared in a glove box. The data were corrected for the sample holder and the diamagnetic contributions calculated from Pascal's constants. The alternating current (AC) magnetic susceptibility measurements were carried out in the presence of a 3 Oe oscillating field in zero or applied external DC field.

Photoluminescence measurements

All spectroscopic measurements as well as the luminescence quantum yield (Q_{Ln}^L) were conducted at ambient temperature in the crystalline phase on a Horiba Jobin Yvon Fluorolog FL3-22 spectrofluorimeter. A 450 W xenon lamp emitting within the 250-900 nm spectral range was employed as the excitation source. The luminescence of the samples was detected with a Hamamatsu R928 photomultiplier operating within 200–850 nm. For the Q_{Ln}^L measurements, a G8 Spectralon®-covered integrating sphere (GMP SA, Switzerland) was mounted inside the spectrofluorimeter. The sample in a quartz vial was placed into the sphere. All Q_{Ln}^L measurements were repeated at least three times to achieve an experimental error below 15%.

To perform variable temperature measurements the custom made setup based on liquid nitrogen vacuum optical cryostat (LN-121-Spectrum liquid N_2 cryostat, Cryotrade Engineering LLC, Russia, equipped with a LakeShore 325 temperature controller (LakeShore, USA) and an HiCube 80 Eco vacuum turbomolecular pump (Pfeiffer Vacuum, Germany) and an Ocean Optics Maya 2000 Pro CCD spectrometer sensitive in the spectral range 200-1100 nm. A 365 nm CW laser source was used for optical excitation. The instrument response function was taken into account.

Results and Discussions

Synthesis and crystal structures

The reactions of $Ln(ClO_4)_3(H_2O)_6$ with 3 equivalents of 2,6-bis(1-methyl-imidazol-2-yl)pyridine (L) in acetonitrile resulted in the complexes with formula $[LnL_3](ClO_4)_3 \cdot H_2O \cdot 2MeCN$ (Ln = Eu (**1**), Tb (**2**), Dy (**3**), Er (**4**), Yb (**5**); Scheme 1). Compounds **1**–**5** were isolated as almost colorless suitable for single-crystal X-ray analysis crystals after the concentration of their solutions in acetonitrile at ambient conditions and were obtained in 65-86% yield. Eu/Tb solid solutions have been synthesized by recrystallization of **1** and **2** with the targeted Eu/Tb ratio. Remarkably, the compounds proved to be hydrolytically and air-stable over several months.

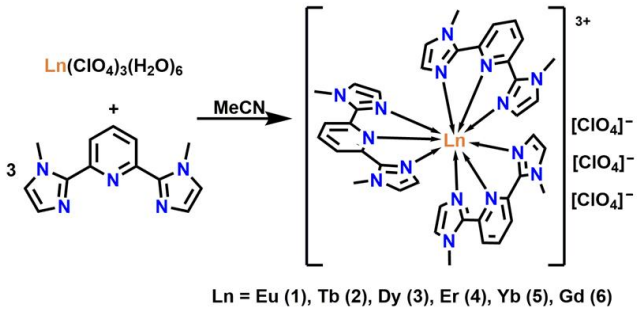

Scheme 1. Synthesis of complexes **1**–**6**.

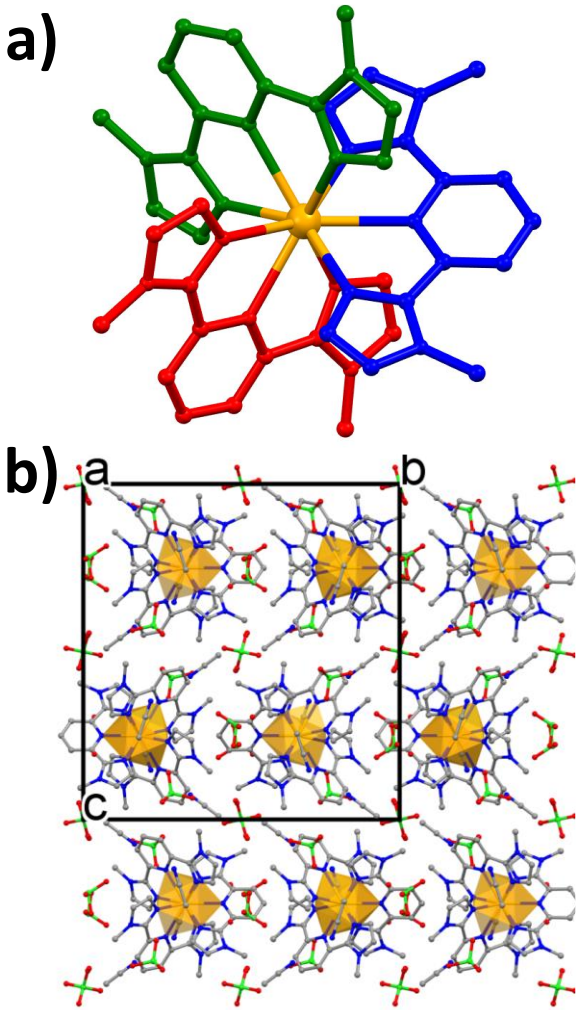

Fig. 1. a) Molecular structure of **3** showing the three-blade propeller generated by three L ligands b) View of the crystal packing for **3** along the *a* crystallographic axis. Color code: orange, Dy; red, O; grey, C; green, Cl. Hydrogen atom have been omitted for clarity.

Table 1: Some structural parameters for compounds **1-5.**

Compound	Ln–$N_{imidazole}$ distances (Å)	Ln–$N_{pyridine}$ distances (Å)	$N_{pyridine}$–Ln–$N_{pyridine}$ angle (°)
1	2.493(3) 2.503(3) 2.510(3)	2.614(3) 2.644(3)	119.4(1) 121.3(1)
2	2.469(3) 2.475(3) 2.482(3)	2.586(3) 2.628(3)	119.28(7) 121.4(1)
3	2.462(3) 2.469(3) 2.474(3)	2.586(3) 2.614(3)	119.4(1) 121.3(1)
4	2.441(3) 2.449(3) 2.458(3)	2.568(3) 2.590(3)	119.25(8) 121.5(1)
5	2.421(7) 2.428(7) 2.438(7)	2.542(8) 2.574(7)	119.2(1) 121.6(3)

Analysis by X-ray diffraction indicates that all compounds crystallize in the orthorhombic achiral *Cmca* space group with half a complex in the asymmetric unit (Table S1). Only the crystal structure of the dysprosium analogue **3** will be described in detail, whereas some relevant crystallographic information could be found in Table 1. The coordination sphere of the Dy^{3+} ion is exclusively constituted by nitrogen atoms originating from three tridentate ligands (L) wrapped around the lanthanide site, giving a coordination number of nine (Figure 1a). A clear helicity could be detected giving rise to an approximate D_3 local symmetry (Figure 1a). Given the achiral space group, the compound is a racemate incorporating an equal amount of Δ and Λ enantiomers (Figure S1). The geometry of the lanthanide site was quantitatively analyzed using the SHAPE software[61] that indicates an intermediate geometry between a tricapped trigonal prism and a spherical capped square antiprism (Table S2). The Dy–N bonds lengths involving the imidazole moieties appear noticeably shorter (2.462(3)–2.474(3) Å) with respect to the Dy–N(pyridine) ones (2.586(3) and 2.614(3) Å) whereas the N(pyridine)-Dy-N(pyridine) are equal to 119.4(1) and 121.3(1)°. Three perchlorate molecules ensure the electroneutrality, while two acetonitrile and two water solvates are also present in the crystal lattice. The packing analysis reveals that perchlorate and solvates form layers in the *bc* plane that separate the complexes (Figure 1b, Figure S2). Hydrogen bonds involving the imidazole moieties, perchlorate, and solvates molecules could be detected while π interactions implying the pyridine ligands with the shortest C–C intermolecular distances of 3.696 Å are also observed. The shortest intermolecular Dy^{3+}–Dy^{3+} distance in the crystal is found to be equal to 10.444 Å.

Magnetic Properties

At the exception of the europium sample, which is known to be diamagnetic at low temperature, the magnetic properties of all samples were investigated in both, static and dynamic modes by using a SQUID MPMS-XL.

The room temperatures χT values of 12.44, 14.45, 12.97 and 3.50 $cm^3 \cdot K \cdot mol^{-1}$ for **2**, **3**, **4**, and **5**, respectively are in a relatively good accordance with the theoretical ones of 11.82, 14.17, 11.48 and 2.57 $cm^3 \cdot K \cdot mol^{-1}$ expected for a unique Ln^{3+} ion using the free-ion approximation (Tb^{3+}, $^7F_6$, $S = 3$, $L = 3$, $g = 3/2$; Dy^{3+},$^6H_{15/2}$, $S = 5/2$, $L = 5$, $g = 4/3$; Er^{3+}, $^4I_{15/2}$, $S = 3/2$, $L = 5$, $g = 6/5$; Yb^{3+},$^2F_{7/2}$, $S = 1/2$, $L = 3$, $g = 8/7$).[62-63] Lowering the temperature induces the typical decrease of χT caused by the thermal depopulation of the m_J levels (Figure 2a) to reach the values of 4.94, 7.00, 5.66 and 1.79 $cm^3 \cdot K \cdot mol^{-1}$ for **2**, **3**, **4**, and **5**, respectively at 1.8 K. The field dependences of the magnetization at this temperature show values of 6.47, 5.97, 5.88 and 1.66 $N\beta$ under a 70 kOe field for **2**, **3**, **4**, and **5**, respectively (Figure 2b).

In order to investigate the occurrence of slow relaxation of the magnetization, alternate currents (AC) measurements were carried out. In the absence of a static DC field, no significant out-of-phase susceptibility χ'' could be detected (Figure S3). This behavior is in line with a strong Quantum Tunnelling of the Magnetization (QTM) due to the low symmetry of the complexes. This is confirmed by *ab initio* calculations at the Complete Active Space Self-Consistent Field (CASSCF) levels performed on **2-5** (see details in the ESI). Such calculations have been extensively used to account the magnetic properties of lanthanide-based SMMs.[6, 64-67] For all the complexes, non-negligible transverse component of the *g* tensor are found for the ground state (Table S3), resulting in a significant QTM. Aiming at shortcutting this QTM, the frequency dependence of the ac susceptibility was investigated in the presence of various dc fields (Figure S3). While the dysprosium and erbium analogues exhibit a weak and broad χ'' component at low frequencies, the Yb complex **5** shows a single peak located at high frequency. As regards the Tb analogue **2**, there is no sign of slow relaxation of the magnetization. Unfortunately, the temperature dependence of the ac susceptibility for **3** and **4** do not show the presence of a χ'' maximum precluding the study of the relaxation dynamics whereas complex **5** exhibits already a maximum close to maximum available frequency (Figure S3), precluding an in-depth study of the relaxation dynamics.

Photoluminescence studies

The tridentate L ligand, coordinated to Ln^{3+} ions might act as an "antenna" to sensitize the lanthanide. The luminescence properties of all samples were therefore investigated in the solid-state at room temperature. At the exception of the erbium analogue **4**, all the samples exhibit the characteristic lanthanide-based luminescence of the related lanthanide ion under optical excitation in the UV (Figures S5-S7).

For the europium complex **1**, the luminescence excitation spectrum monitored at 617 nm, corresponding to the most intense $^5D_0 \rightarrow {}^7F_2$ transition, exhibits a broad band associated with the Eu^{3+} luminescence excitation via π-π* electronic transitions in the ligand environment (Figure S6). These spectral features have a maximum located at about 366 nm. The broadness of this band indicates a main excitation through the L ligand. In contrast, direct sensitization through the *f-f* transitions would give sharp lines in the excitation spectrum.[68]

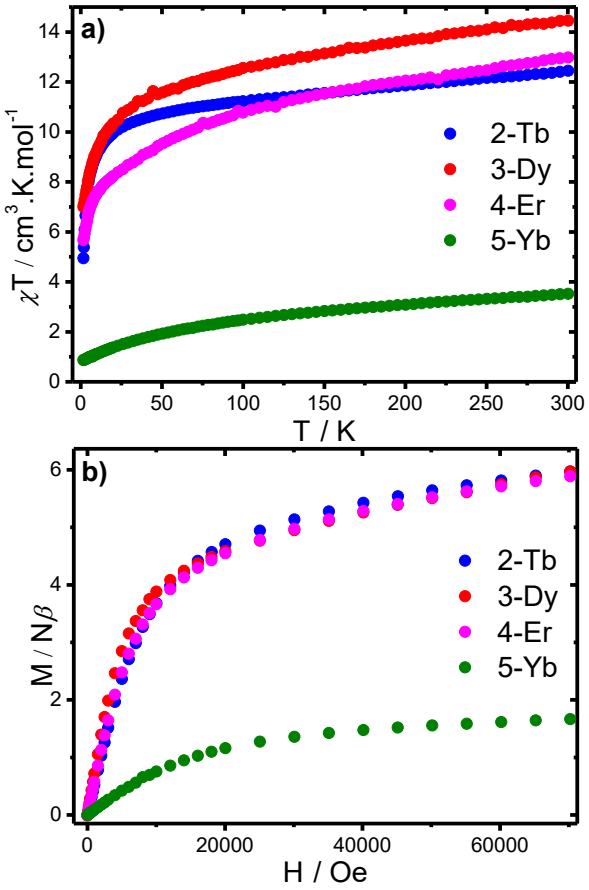

Fig. 2: a) Temperature dependence of χT under an applied magnetic field of 1000 Oe for **2–5**. b) Field dependence of the magnetization at 1.8 K for **2–5**.

Upon excitation at 366 nm, **1** exhibits emission bands centered at 581, 593, 617 (with sub-bands centered at 619 and 628 nm), 650, and 689 (with sub-bands centered at 695 and 703 nm) that could be assigned to the 4*f*-4*f* transitions of the Eu^{3+} ion, namely $^5D_0 \rightarrow {}^7F_J$ (J = 0, 1, 2, 3, 4), respectively (Figure 3a).

As it can be seen from Figure 3b, the Tb complex **2** displays the typical terbium luminescence with emission peaks at 489, 544, 582, 620, 645, 666, and 676 nm, assigned to $^5D_4 \rightarrow {}^7F_J$ (J = 6, 5, 4, 3, 2, 1, and 0) transitions, respectively. The excitation spectrum monitored in the $^5D_4 \rightarrow {}^7F_5$ transition (544 nm) shows several broad bands located within 300-350, 360-420, and 420-460 nm which can be connected to π-π* electronic transitions related to the L ligand whereas a sharp line at 488 nm could be assigned to the $^7F_6 \rightarrow {}^5D_4$ transition (see Figure S6).

We also observed photoluminescence for the dysprosium complex **3**. The obtained spectra reveal the characteristic Dy^{3+} ion emission peaks centered at 480 nm ($^4F_{9/2} \rightarrow {}^6H_{15/2}$), 574 nm ($^4F_{9/2} \rightarrow {}^6H_{13/2}$), and 663 nm ($^4F_{9/2} \rightarrow {}^6H_{11/2}$) and ligand centered emission (see Figure 3c).

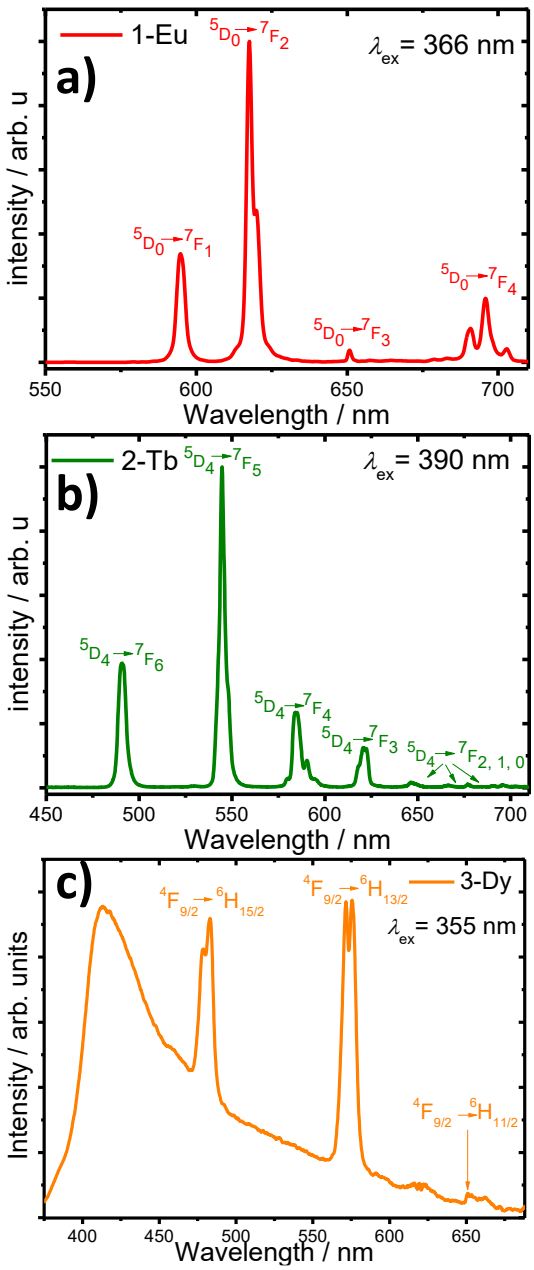

Fig. 3: Emission spectra of complexes Eu **1** (a), Tb **2** (b) and Dy **3** (c).

The spectral band corresponding to the ligand luminescence is spawned up to 670 nm with a maximum at 420 nm, suggesting the incomplete energy transfer from ligand to Dy^{3+} ion. This is confirmed by theoretical calculations on energy transfer, where the backward energy transfer $Dy^{3+} \rightarrow T_1$ dominates the process (three times higher than the forward $T_1 \rightarrow Dy^{3+}$, see section *S2.4 Ligand-to-Ln^{3+} energy transfer* in Supporting Information).

We can however not observe any metal-centered photoluminescence for compound **4,** as frequently seen for erbium complexes whereas the ytterbium complex **5** exhibits only weak photoluminescence in the NIR region corresponding to the $^2F_{5/2} \rightarrow {}^2F_{7/2}$ transition when excited at 396 nm (Figure S7b). Two distinct shoulders could be observed at 980 nm and 1000 nm, respectively which corresponds to the splitting of the Stark components. The excitation spectrum monitored at 980 nm points out a sensitization by the L ligand with a large band showing a maximum at 396 nm. The weakness of the emission intensity points out however a modest sensitization of the ligands towards the Yb^{3+} ion.

While the probability of the energy transfer rate is directly connected with the energy difference between donor and acceptor states, one needs to obtain the energy of the first excited triplet state of the L ligand. Since the vibration motions are mainly «frozen» at cryogenic temperatures (77 K), the triplet state energy of the ligand can be estimated from the high-energy band (0–0 phonon transition) observed in the phosphorescence spectra for the Gd complex **6** (see Figure S7c), which was synthesized for this purpose. Yet, the 0–0 transition energy is higher than the peak of the high-energy band of emission due to the reorganization

of the radiation energy.[69] Thus, the triplet state T_1 energy can be evaluated from the high-energy edge of the phosphorescence spectrum. We estimated the position of the lowest triplet state as 21900 cm^{-1}.

To get further insights into the energy relaxation processes, photoluminescence decays were recorded by monitoring the maxima of their emission under pulsed laser excitation at 355 nm. The obtained decays revealed single-exponential behavior (see Figure S8) and can be well-fitted using an appropriate single-exponential model. Characteristic lifetimes were estimated as 1.86 ms for complex **1** (Eu), 245 µs for **2** (Tb) and 55 µs for **3** (Dy), confirming the low sensitization efficiency of the Tb^{3+} and Dy^{3+} ion luminescence. The lifetimes measured for complexes **1**–**3** are typical values for europium, terbium, and dysprosium complexes,[10-11, 70-72] and are in argument with an energy transfer involving the first excited triplet state T_1 of the L ligand and therefore with the Latva's rule.[73]

The overall luminescence quantum yields (Q_{Ln}^{L}) were measured by the absolute method for complexes **1** and **2**. We obtained a relatively high value of $Q_{Eu}^{L} = 0.57$ for europium analogue whereas a modest value of $Q_{Tb}^{L} = 0.17$ is found for the terbium complex.

Remarkably, theoretical calculations (see Supporting Information for complete details) through time-dependent density functional theory (TD-DFT) using B3LYP/6-31(Gd)/MWB52(Eu)/MWB54(Tb),[74-76] intramolecular energy transfer (IET),[14, 77] and rate equations modeling[14, 78] allow to simulate the Q_{Ln}^{L} as a function of unknown decay parameters such as the T_1 and S_1 decay lifetimes (τ_T and τ_S) and the $S_1 \rightarrow T_1$ intersystem crossing rate (W_{ISC}), as shown in Figure S14 and Figure 4. The emission quantum yield Q_{Ln}^{L} showed a poor dependence with the τ_T (Figure S14) due to an effective energy transfer from the $T_1 \rightarrow Ln^{3+}$ (W^T in Tables S5 and S6), mathematically this means that $W^T > 1/\tau_T$ at 300 K.

Once we are dealing with Ln^{3+}-based compounds experiencing the same structural and chemical environment features, the rates $1/\tau_T$, $1/\tau_S$, and W_{ISC} should not vary so much when the Ln^{3+} is changed as they are more related to the electronic structure of the ligands.

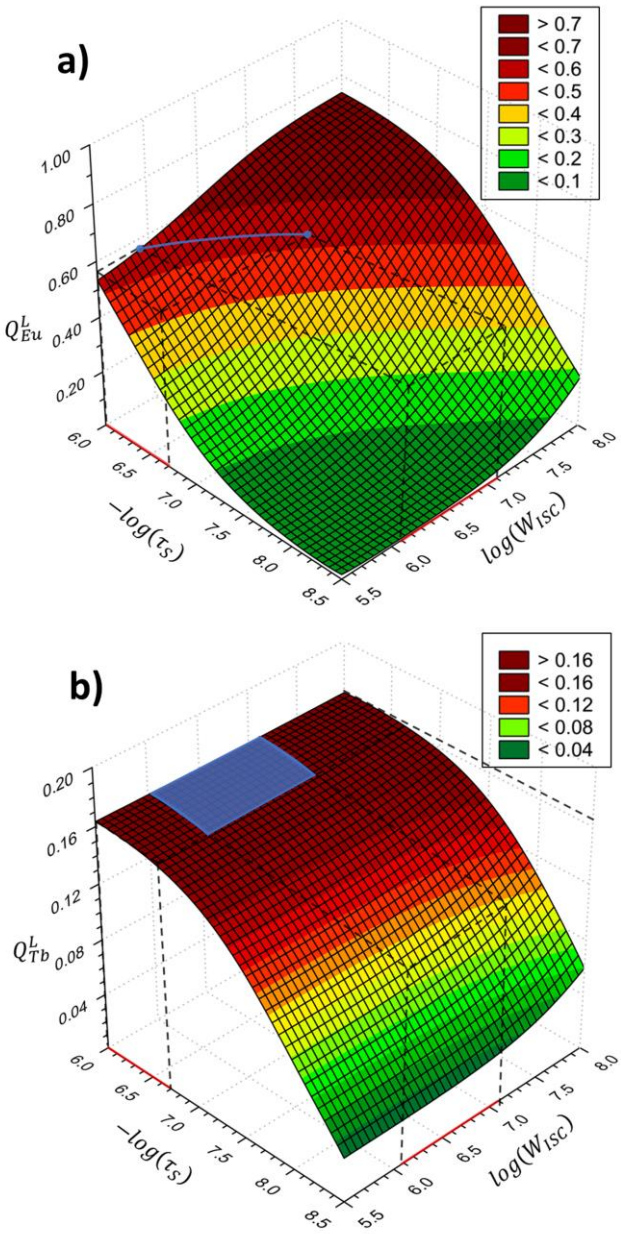

Fig. 4. Emission quantum yields Q^L_{Ln} for complexes a) **1** and b) **2** as a function of the S_1 decay lifetime (τ_S) and the $S_1 \rightarrow T_1$ intersystem crossing rate (W_{ISC}). The intervals highlighted in red at the axis represent the reasonable values of τ_S and W_{ISC} which the Q^L_{Ln} is closer to the experimental ones ($Q^L_{Eu} = 0.57$ and $Q^L_{Tb} = 0.17$). $\tau_T = 10^{-4}$ s was fixed in both simulations. A total of 225 points of calculated Q^L_{Ln} for each complex were used to generate the surfaces. The data were statistically treated by the weighted least squares method.

Obviously, in the presence of the Ln^{3+} ion, the heavy atom effect has a strong influence on the spin-orbit coupling, causing a mixture of the singlet and triplet states which is responsible for the τ_T and τ_S lifetimes changing.[79-80] Also, the $S_1 \rightarrow T_1$ intersystem crossing W_{ISC} is proportional to the square of the spin-orbit coupling matrix elements $\langle S_1|H_{SO}|T_1\rangle$ and inversely proportional to the energy gap between S_1 and T_1 states ΔE_{S-T}, $W_{ISC} \propto \langle S_1|H_{SO}|T_1\rangle^2 e^{-(\Delta E_{S-T})^2}$.[81] Thus, upon modulating the Ln^{3+} ion, the $1/\tau_T$, $1/\tau_S$, and W_{ISC} will be practically the same for Ln^{3+} analogous complexes. In this manner, we can use the measured emission quantum yields for complexes **1** and **2** as references to estimate the τ_T, τ_S, and W_{ISC} within acceptable physical values (τ_T from 10^{-3} to 10^{-6} s, τ_S from 10^{-6} to 10^{-9} s, and W_{ISC} from 10^5 to 10^8 s^{-1} considering the $\Delta E_{S-T} = 4980$ cm^{-1}) for Ln-based complexes,[82] otherwise, the theoretical Q^L_{Ln} becomes meaningless (*e.g.* $\tau_T \ll \tau_S$ will drop all Q^L_{Ln} to zero).

Luminescence thermometry

Both, Eu and Tb complexes exhibiting typical lanthanide luminescence open interesting perspectives for the design of mixed Eu/Tb complexes which could act as self-referencing molecular thermometers in solid-state. The temperature-dependent

photoluminescence measurements for different Eu/Tb ratios (1:10, 1:1, 5:1) were conducted at a temperature range 77–300 K. In the case of $Eu_{0.09}Tb_{0.91}$, an increase of the Tb^{3+} emission contribution in the spectrum could be observed when lowering the temperature from 298 to 77 K (see Figure 5). Thus, the emission color monotonically changes from red to yellow-green as demonstrated by the points on CIE (Commision Internationale de l'éclairage) chromaticity diagram (see Figure 6). We also observed linear dependence of *y* or *x* CIE coordinates with a slope coefficient 0.90 (R^2 = 0.99). This demonstrates the possibility of finely tuning the emission color. On the other hand, for the other Eu/Tb ratios, this effect is less pronounced (see Figure S9). In the next, we will therefore focus on the $Eu_{0.09}Tb_{0.91}$ sample.

The thermal dependence of the emission colour could be viewed as an advantage to employ such complexes as molecular thermometers. Hence, the ratiometric parameter Δ was estimated by calculating the ratio of the integrated intensities corresponding to the $^5D_4 \rightarrow {}^7F_5$ transition of Tb^{3+} and the $^5D_0 \rightarrow {}^7F_4$ of Eu^{3+} ions. The temperature dependence of the ratiometric parameter Δ was also modeled using theoretical methods described by Carneiro Neto *et al.*[55] and in the Supporting Information.

The relative thermal sensitivity and minimum temperature uncertainty are defined as:[83]

$$S_r = \frac{1}{\Delta}\left|\frac{\partial \Delta}{\partial T}\right| \quad (1)$$

$$\delta T = \frac{1}{S_r}\frac{\delta \Delta}{\Delta} \quad (2)$$

where $\delta\Delta$ is the uncertainty in Δ. It reveals that the thermometric operating range for **$Eu_{0.09}Tb_{0.91}$** is ranging between 95–225 K where Δ decreases (see Figure 7). In this region, the thermal sensitivity starts from 0.1 %·K^{-1} at 95 K with a maximum 6.6% K^{-1} in the 150-170 K interval. The uncertainty grows together with the temperature, but it is still not higher than 0.1 K below 180 K (see Figure S15). Consequently, the investigated compound **$Eu_{0.09}Tb_{0.91}$** has the best thermometric performance at T_m = 160 K with S_r = 6.6%·K^{-1} and δT = 0.038 K. For comparison, lower sensitivity is achieved for **$Eu_{0.09}Tb_{0.91}$** due to the saturation of Δ parameter bellow 130 K. The maximum observed S_r value is comparable to the values reported in the literature for mixtures of Eu^{3+} and Tb^{3+} complexes operating in this temperature range (Table S4).[34, 54-55, 84]

In order to get further insights, we use our theoretical model to describe the thermometric behavior of the mixed compounds by analyzing the individual Eu and Tb complexes **1** and **2**. Indeed, the large intermolecular Ln-Ln distances implies that the kinetics of the $Tb^{3+} \rightarrow Eu^{3+}$ transfer could be neglected. This is supported by the luminescence decay curve of the mixed $Eu_{0.09}Tb_{0.91}$ complex (Figure S16), monitored at the Eu^{3+} $^5D_0 \rightarrow {}^7F_2$ transition, which reveals a single-exponential behavior and no rise. This indicates that there is no significant Tb^{3+}-to-Eu^{3+} energy transfer due to the long long-distance between the Ln^{3+} ions.[49, 55, 85-86]

Compound **1** is very sensitive to the relative population growth of the $^7F_1$ level when the temperature increases,[14, 49, 87] although the highest contribution of energy transfer is due to $T_1 \rightarrow [{}^7F_0 \rightarrow {}^5D_1]$ by the exchange mechanism (see pathway 17 in Table S6).

For compound **2**, the energy transfer occurs predominantly via $S_1 \rightarrow Tb^{3+}$ and this reflects the small dependence of the quantum yield with the ISC (Figure 3b) once the $T_1 \rightarrow Tb^{3+}$ is less operative. Pathways $S_1 \rightarrow [{}^7F_6 \rightarrow {}^5G_6]$ and $S_1 \rightarrow [{}^7F_5 \rightarrow {}^5G_5]$ (Table S7) are the dominant ones due to their good energy resonance conditions and high values of reduced matrix elements of the spin operator $\langle {}^7\boldsymbol{F_6}||\boldsymbol{S}||{}^5\boldsymbol{G_6}\rangle = \boldsymbol{0.555}$ and $\langle {}^7\boldsymbol{F_5}||\boldsymbol{S}||{}^5\boldsymbol{G_5}\rangle = \boldsymbol{0.243}$ (in units of $\hbar$).[88] Despite the fact that the Tb^{3+} $^7F_5$ level is not thermally coupled with the $^7F_6$, as in the case of the Eu^{3+} for $^7F_1$ and $^7F_0$ ones, the $^7F_5$ level is considered in our calculations due to its long decay time.[89-90] Previous studies pointed out the importance of this level in the IET process.[88, 91-93] In particular, Kasprzycka *et al.* carried out a study on the complex $Na[Tb(L)_4]$ (H–L = dimethyl(4-methylphenylsulfonyl)amidophosphate) and the authors showed that if the $^7F_5$ is not considered in the IET process as an initial acceptor level, the calculated $\boldsymbol{Q_{Tb}^L}$ drops from 0.57 to 0.015%, while the measured $\boldsymbol{Q_{Tb}^L}$ one is 0.58.[92]

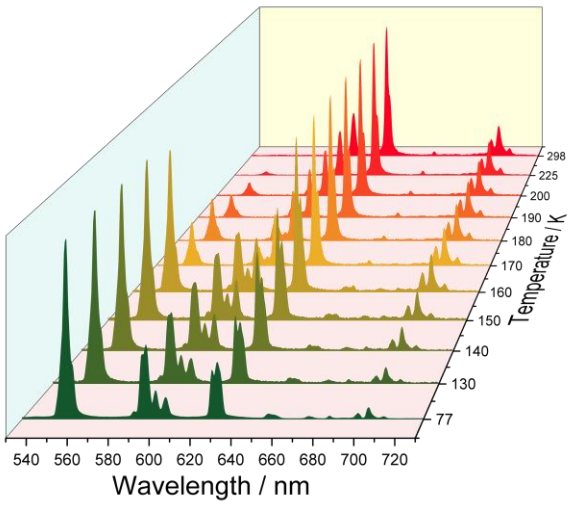

Fig. 5. Emission spectrum of the mixed Eu-Tb complex **$Eu_{0.09}Tb_{0.91}$** at different temperatures.

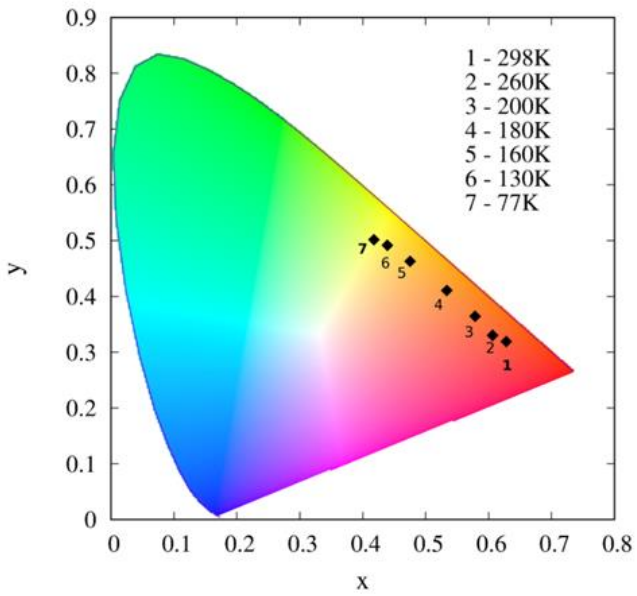

Fig. 6. CIE chromaticity coordinates for the $\mathbf{Eu_{0.09}Tb_{0.91}}$ mixed complex at different temperatures.

Thus, whereas the terbium complex exhibits a dominant $S_1 \rightarrow Tb^{3+}$ IET, the situation with europium complex is reversed and involved mostly a $T_1 \rightarrow Eu^{3+}$ pathway. Once all rates involved in the Jablonski-type diagrams for compounds **1** and **2** (Figure S12a,b) are obtained, we constructed an appropriate rate equation model (Eqs. S15–S19) to determine the Tb^{3+} $^5D_4$ and the Eu^{3+} $^5D_0$ emitting levels population fractions (labeled as $\boldsymbol{P_4}$). These quantities together with the radiative rates (obtained using the JOYSpectra program[94]) of $^5D_4 \rightarrow {}^7F_5$ and $^5D_0 \rightarrow {}^7F_4$ transitions provide the intensities $\boldsymbol{I_{Tb}}$ and $\boldsymbol{I_{Eu}}$ and consequently the theoretical thermometric parameter (Eq. S8). As shown in Figure 7, our methodology allows to reproduce nicely the thermal dependence of the thermometric parameter Δ and the relative sensitivity $\boldsymbol{S_r}$ in the mixed $\mathbf{Eu_{0.09}Tb_{0.91}}$ complex. We would like to emphasize that this constitutes one of the rare examples in which the thermometric performances were modelled.[55] We point out that they were modelled considering how individual Tb^{3+} and Eu^{3+} complexes may emit ($\Delta = I_{Tb}/I_{Eu}$) as the intermolecular $Tb^{3+} \rightarrow Eu^{3+}$ transfer could be neglected. This thermometric parameter depends however on the number of excited Tb and Eu complexes which, in turn, are related to the concentration of these ions in the sample. This explains why, in this series, the thermometric performances depend on the Eu/Tb ratio of the mixed complexes.

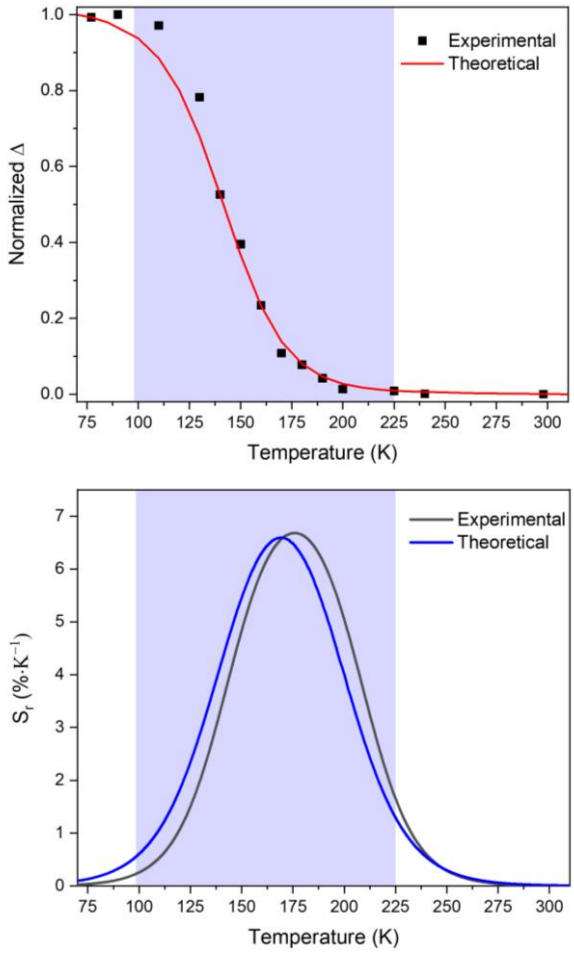

Fig. 7. Top – The $^5D_4 \rightarrow {}^7F_5/{}^5D_0 \rightarrow {}^7F_4$ ratio calculated for the mixed **$Eu_{0.09}Tb_{0.91}$** complex. The shadowed areas show the regions of the so-called operating range. Bottom – Relative thermal sensitivity for the same compound.

Conclusions

We have reported here a series isostructural homoleptic three-blade propeller lanthanide complexes based on the relatively unexplored tridentate 2,6-bis(1-methyl-imidazol-2-yl)pyridine L ligand. The obtained nine-coordinate complexes are chiral but crystallize as racemates. The complexes are stable under aerobic conditions over a long period time both in solid state and solution. The crystals can be readily solubilized in common organic solvents. Magnetic analyses indicate the absence of a clear slow relaxation of the magnetization for all complexes due to the absence of suitable crystal-field necessary to increase the magnetic anisotropy. Yet, the tridentate L ligand appears suitable to sensitize lanthanide ions. Hence, apart from the erbium analogue, the typical Ln^{3+}-based luminescence is observed for all complexes in the series.

In this sense, the mixed Eu/Tb complexes can be used as solid-state ratiometric thermometers in the temperature range 130–220 K. Complex with the metal ratio 1:10 (Eu/Tb) was found to be the most thermally sensitive with the maximum value of S_r = 6.6 %·K^{-1} within the range of 150–170 K. To our knowledge this corresponds to one of the first examples of three-propeller lanthanide complex designed for luminescence thermometry.

Theoretical calculations allow to provide a complete picture of the luminescence mechanisms in the pure complexes including their QY, allowing in turn to model the thermometric performances of the mixed Eu/Tb thermometer. All together, these molecular thermometers behave as sensitive cryogenic thermometer in the solid-state which could be relevant for applications requiring to remotely measure to the temperature. Even though thermometers operating close to room temperature are particularly relevant in terms of applications, cryogenic thermometry appears important across various areas spanning from engineering metallurgy to aerospatial industry.[51-52] Indeed, the common sensors used for cryogenic thermometry are resistors, diodes or thermocouples. They have however a large size and require to be in physical contact with the sensed object. Development of sensors able to remotely and locally measure the temperature might circumvent the aforementioned issues. With respect to some molecular thermometers incorporating water in the lanthanide coordination sphere, the strongly coordinated tridentate L ligand protects the lanthanide from such influence. Besides, the great tunability of such tridentate ligands in terms of steric and electronic features may be taken as an advantage to enhancing the photoluminescence properties. Lastly, the great processability of these complexes implied that these could start as starting materials to engineer future devices.

Conflicts of Interest

There are no conflicts to declare.

Acknowledgements

The financial support of the Russian Science Foundation is highly acknowledged (Project № 17-73-30036-П). The French authors thank the University of Montpellier, CNRS and PAC of ICGM. J. Long also acknowledges the support from the Institut Universitaire de France. Luminescence data were collected using the equipment of the Center for molecular composition studies of INEOS RAS. A. N. Carneiro Neto and L. D. Carlos thank the financial support from the European Union's Horizon 2020 FET Open program under grant agreement no. 801305. This work was also developed within the scope of the project CICECO-Aveiro Institute of Materials, UIDB/50011/2020, UIDP/50011/2020 & LA/P/0006/2020, financed by Portuguese funds through the FCT/MEC (PIDDAC).

Notes and references

1 J. Long, Y. Guari, R. A. S. Ferreira, L. D. Carlos and J. Larionova, Recent advances in luminescent lanthanide based Single-Molecule Magnets, *Coord. Chem. Rev.*, 2018, **363**, 57-70.
2 L. Ungur and L. F. Chibotaru, Strategies toward High-Temperature Lanthanide-Based Single-Molecule Magnets, *Inorg. Chem.*, 2016, **55**, 10043-10056.
3 J.-L. Liu, Y.-C. Chen and M.-L. Tong, Symmetry strategies for high performance lanthanide-based single-molecule magnets, *Chem. Soc. Rev.*, 2018, **47**, 2431-2453.
4 J. Tang and P. Zhang, in *Lanthanide Single Molecule Magnets*, Springer Berlin Heidelberg, Berlin, Heidelberg, 2015, DOI: 10.1007/978-3-662-46999-6_2, pp. 41-90.
5 R. A. Layfield and M. Murugesu, *Lanthanides and Actinides in Molecular Magnetism*, Wiley, 2015.
6 C. A. P. Goodwin, F. Ortu, D. Reta, N. F. Chilton and D. P. Mills, Molecular magnetic hysteresis at 60 kelvin in dysprosocenium, *Nature*, 2017, **548**, 439-442.
7 F.-S. Guo, B. M. Day, Y.-C. Chen, M.-L. Tong, A. Mansikkamäki and R. A. Layfield, Magnetic hysteresis up to 80 kelvin in a dysprosium metallocene single-molecule magnet, *Science*, 2018, **362**, 1400-1403.
8 J.-C. G. Bunzli and C. Piguet, Taking advantage of luminescent lanthanide ions, *Chem. Soc. Rev.*, 2005, **34**, 1048-1077.
9 J. C. G. Bünzli and S. V. Eliseeva, Intriguing aspects of lanthanide luminescence, *Chem. Sci.*, 2013, **4**, 1939-1949.
10 J.-C. G. Bünzli and S. V. Eliseeva, in *Lanthanide Luminescence: Photophysical, Analytical and Biological Aspects*, eds. P. Hänninen and H. Härmä, Springer Berlin Heidelberg, Berlin, Heidelberg, 2011, DOI: 10.1007/4243_2010_3, pp. 1-45.
11 S. V. Eliseeva and J.-C. G. Bünzli, Lanthanide luminescence for functional materials and bio-sciences, *Chem. Soc. Rev.*, 2010, **39**, 189-227.
12 J.-C. G. Bünzli and C. Piguet, Taking advantage of luminescent lanthanide ions, *Chem. Soc. Rev.*, 2005, **34**, 1048-1077.
13 J.-C. G. Bünzli, On the design of highly luminescent lanthanide complexes, *Coord. Chem. Rev.*, 2015, **293-294**, 19-47.
14 A. N. Carneiro Neto, E. E. S. Teotonio, G. F. de Sá, H. F. Brito, J. Legendziewicz, L. D. Carlos, M. C. F. C. Felinto, P. Gawryszewska, R. T. Moura, R. L. Longo, W. M. Faustino and O. L. Malta, in *Handbook on the Physics and Chemistry of Rare Earths*, eds. J.-C. G. Bünzli and V. K. Pecharsky, Elsevier, 2019, vol. 56, pp. 55-162.
15 Y. H. Pham, V. A. Trush, A. N. Carneiro Neto, M. Korabik, J. Sokolnicki, M. Weselski, O. L. Malta, V. M. Amirkhanov and P. Gawryszewska, Lanthanide complexes with N-phosphorylated carboxamide as UV converters with excellent emission quantum yield and single-ion magnet behavior, *J. Mater. Chem. C*, 2020, **8**, 9993-10009.
16 P. A. Brayshaw, J.-C. G. Buenzli, P. Froidevaux, J. M. Harrowfield, Y. Kim and A. N. Sobolev, Synthetic, Structural, and Spectroscopic Studies on Solids Containing Tris(dipicolinato) Rare Earth Anions and Transition or Main Group Metal Cations, *Inorg. Chem.*, 1995, **34**, 2068-2076.
17 E. Huskowska and J. P. Riehl, Perturbation of the Racemic Equilibrium between D3 Lanthanide Complexes through the Addition of Sugars, *Inorg. Chem.*, 1995, **34**, 5615-5621.
18 T. N. Parac-Vogt, K. Binnemans and C. Görller-Walrand, Absolute Configuration Assignment of D3-Symmetric Lanthanide Complexes Based on Circular Dichroism Induced by Interaction with a Chiral Probe, *ChemPhysChem*, 2001, **2**, 767-769.
19 G. Muller and J. P. Riehl, Use of Induced Circularly Polarized Luminescence (CPL) from Racemic D3 Lanthanide Complexes to Determine the Absolute Configuration of Amino Acids, *J. Fluoresc.*, 2005, **15**, 553-558.
20 K. Staszak, K. Wieszczycka, V. Marturano and B. Tylkowski, Lanthanides complexes – Chiral sensing of biomolecules, *Coord. Chem. Rev.*, 2019, **397**, 76-90.
21 C. Piguet, A. F. Williams, G. Bernardinelli and J. C. G. Buenzli, Structural and photophysical properties of lanthanide complexes with planar aromatic tridentate nitrogen ligands as luminescent building blocks for triple-helical structures, *Inorg. Chem.*, 1993, **32**, 4139-4149.
22 H.-R. Mürner, E. Chassat, R. P. Thummel and J.-C. G. Bünzli, Strong enhancement of the lanthanide-centred luminescence in complexes with 4-alkylated 2,2';6',2''-terpyridines*J. Chem. Soc., Dalton Trans.*, 2000, DOI: 10.1039/B003577G, 2809-2816.
23 S. Petoud, J.-C. G. Bünzli, T. Glanzman, C. Piguet, Q. Xiang and R. P. Thummel, Influence of charge-transfer states on the Eu(III) luminescence in mononuclear triple helical complexes with tridentate aromatic ligands, *J. Lumin.*, 1999, **82**, 69-79.
24 D. Zare, Y. Suffren, L. Guénée, S. V. Eliseeva, H. Nozary, L. Aboshyan-Sorgho, S. Petoud, A. Hauser and C. Piguet, Smaller than a nanoparticle with the design of discrete polynuclear molecular complexes displaying near-infrared to visible upconversion, *Dalton Trans.*, 2015, **44**, 2529-2540.

25 Y. Li, J. C. Huffman and A. H. Flood, Can terdentate 2,6-bis(1,2,3-triazol-4-yl)pyridines form stable coordination compounds?, *Chem. Commun.*, 2007, DOI: 10.1039/B703301J, 2692-2694.
26 A. Bhattacharyya, P. M. Forster, D. B. Rego and K. R. Czerwinski, Lanthanide Complexation of 2,6-Bis(5,6-dipyridyl-1,2,4-triazinyl)pyr-idine – Solvent- and Lanthanide-Ion-Controlled Ligand Coordination Mode and Denticity, *Eur. J. Inorg. Chem.*, 2016, **2016**, 921-927.
27 J.-R. Jiménez, I. F. Díaz-Ortega, E. Ruiz, D. Aravena, S. J. A. Pope, E. Colacio and J. M. Herrera, Lanthanide Tetrazolate Complexes Combining Single-Molecule Magnet and Luminescence Properties: The Effect of the Replacement of Tetrazolate N3 by β-Diketonate Ligands on the Anisotropy Energy Barrier, *Chem. Eur. J.*, 2016, **22**, 14548-14559.
28 S. Di Pietro, N. Gautier, D. Imbert, J. Pécaut and M. Mazzanti, Versatile pyridine-2,6-bis-tetrazolate scaffolds for the formation of highly luminescent lanthanide complexes, *Dalton Trans.*, 2016, **45**, 3429-3442.
29 Y.-W. Yip, H. Wen, W.-T. Wong, P. A. Tanner and K.-L. Wong, Increased Antenna Effect of the Lanthanide Complexes by Control of a Number of Terdentate N-Donor Pyridine Ligands, *Inorg. Chem.*, 2012, **51**, 7013-7015.
30 D. A. Bardwell, J. C. Jeffery, P. L. Jones, J. A. McCleverty, E. Psillakis, Z. Reeves and M. D. Ward, Lanthanide complexes of the tetradentate N-donor ligand dihydrobis[3-(2-pyridyl)pyrazolyl]borate and the terdentate N-donor ligand 2,6-bis(1H-pyrazol-3-yl)pyridine: syntheses, crystal structures and solution structures based on luminescence lifetime studies, *J. Chem. Soc., Dalton Trans.*, 1997, DOI: 10.1039/A701297G, 2079-2086.
31 R. F. Carina, G. Bernardinelli and A. F. Williams, Structure of a One-Dimensional Infinite Double-Helical Copper(I) Complex, *Angew. Chem. Int. Ed.*, 1993, **32**, 1463-1465.
32 R. F. Carina, A. F. Williams and C. Piguet, Stability and Lability of Dicopper Double-Stranded Helicates in Solution, *Helv. Chim. Acta*, 1998, **81**, 548-557.
33 S. W. Allison, A brief history of phosphor thermometry, *Meas. Sci. Technol.*, 2019, **30**, 072001.
34 C. D. S. Brites, S. Balabhadra and L. D. Carlos, Lanthanide-Based Thermometers: At the Cutting-Edge of Luminescence Thermometry, *Adv. Opt. Mater.*, 2019, **7**, 1801239.
35 D. Jaque and F. Vetrone, Luminescence nanothermometry, *Nanoscale*, 2012, **4**, 4301-4326.
36 C. D. S. Brites, P. P. Lima, N. J. O. Silva, A. Millán, V. S. Amaral, F. Palacio and L. D. Carlos, Thermometry at the nanoscale, *Nanoscale*, 2012, **4**, 4799-4829.
37 C. D. S. Brites, A. Millán and L. D. Carlos, in *Handbook on the Physics and Chemistry of Rare Earths*, eds. J.-C. G. Bünzli and V. K. Pecharsky, Elsevier Science, B. V., Amsterdam, 2016, vol. 49, ch. 281, pp. 339-427.
38 Y. Cheng, Y. Gao, H. Lin, F. Huang and Y. Wang, Strategy Design for Ratiometric Luminescence Thermometry: Circumventing the Limitation of Thermally Coupled Levels, *J. Materials Chemsitry C*, 2018, **6**, 7462-7478.
39 M. C. Jia, Z. Sun, M. X. Zhang, H. Y. Xu and Z. L. Fu, What determines the performance of lanthanide-based ratiometric nanothermometers?, *Nanoscale*, 2020, **12**, 20776-20785.
40 E. J. McLaurin, L. R. Bradshaw and D. R. Gamelin, Dual-Emitting Nanoscale Temperature Sensors, *Chem. Mater.*, 2013, **25**, 1283-1292.
41 C. D. S. Brites, K. Fiaczyk, J. F. C. B. Ramalho, M. Sójka, L. D. Carlos and E. Zych, Widening the Temperature Range of Luminescent Thermometers through the Intra- and Interconfigurational Transitions of Pr3+, *Adv. Opt. Mater.*, 2018, **6**, 1701318.
42 M. Suta and A. Meijerink, A Theoretical Framework for Ratiometric Single Ion Luminescent Thermometers—Thermodynamic and Kinetic Guidelines for Optimized Performance, *Adv. Theory Simul.*, 2020, **3**, 2000176.
43 M. Back, J. Ueda, H. Nambu, M. Fujita, A. Yamamoto, H. Yoshida, H. Tanaka, M. G. Brik and S. Tanabe, Boltzmann Thermometry in Cr3+-Doped Ga2O3 Polymorphs: The Structure Matters!, *Adv. Opt. Mater.*, 2021, **n/a**, 2100033.
44 E. C. Ximendes, W. Q. Santos, U. Rocha, U. K. Kagola, F. Sanz-Rodriguez, N. Fernandez, A. D. Gouveia-Neto, D. Bravo, A. M. Domingo, B. del Rosal, C. D. S. Brites, L. D. Carlos, D. Jaque and C. Jacinto, Unveiling in Vivo Subcutaneous Thermal Dynamics by Infrared Luminescent Nanothermometers, *Nano Letters*, 2016, **16**, 1695-1703.
45 A. M. Kaczmarek, Y.-Y. Liu, M. K. Kaczmarek, H. Liu, F. Artizzu, L. D. Carlos and P. Van Der Voort, Developing Luminescent Ratiometric Thermometers Based on a Covalent Organic Framework (COF), *Angew. Chem. Int. Ed.*, 2020, **59**, 1932-1940.
46 C. D. S. Brites, P. P. Lima, N. J. O. Silva, A. Millán, V. S. Amaral, F. Palacio and L. D. Carlos, A Luminescent Molecular Thermometer for Long-Term Absolute Temperature Measurements at the Nanoscale, *Adv. Mater.*, 2010, **22**, 4499-4504.
47 A. Cadiau, C. D. S. Brites, P. M. F. J. Costa, R. A. S. Ferreira, J. Rocha and L. D. Carlos, Ratiometric Nanothermometer Based on an Emissive Ln^{3+}-Organic Framework, *Acs Nano*, 2013, **7**, 7213-7218.
48 R. Piñol, C. D. S. Brites, R. Bustamante, A. Martínez, N. J. O. Silva, J. L. Murillo, R. Cases, J. Carrey, C. Estepa, C. Sosa, F. Palacio, L. D. Carlos and A. Millán, Joining Time-Resolved Thermometry and Magnetic-Induced Heating in a Single Nanoparticle Unveils Intriguing Thermal Properties, *ACS Nano*, 2015, **9**, 3134-3142.
49 V. Trannoy, A. N. Carneiro Neto, C. D. S. Brites, L. D. Carlos and H. Serier-Brault, Engineering of Mixed Eu3+/Tb3+ Metal-Organic Frameworks Luminescent Thermometers with Tunable Sensitivity, *Adv. Opt. Mater.*, 2021, **9**, 2001938.
50 T. P. van Swieten, D. Yu, T. Yu, S. J. W. Vonk, M. Suta, Q. Zhang, A. Meijerink and F. T. Rabouw, A Ho3+-Based Luminescent Thermometer for Sensitive Sensing over a Wide Temperature Range, *Adv. Opt. Mater.*, 2021, **9**, 2001518.
51 M. D. Dramićanin, Trends in luminescence thermometry, *J. Appl. Phys.*, 2020, **128**, 040902.
52 H. Suo, X. Zhao, Z. Zhang, Y. Wang, J. Sun, M. Jin and C. Guo, Rational Design of Ratiometric Luminescence Thermometry Based on Thermally Coupled Levels for Bioapplications, *Laser Photonics Rev.*, 2021, **15**, 2000319.
53 K. Li and R. Van Deun, Site-Bi3+ and Eu3+ dual emissions in color-tunable Ca2Y8(SiO4)6O2:Bi3+, Eu3+ phosphors prepared via sol-gel synthesis for potentially ratiometric temperature sensing, *J. Alloys Compd.*, 2019, **787**, 86-95.
54 Q. Wang, M. Liao, Q. Lin, M. Xiong, Z. Mu and F. Wu, A review on fluorescence intensity ratio thermometer based on rare-earth and transition metal ions doped inorganic luminescent materials, *J. Alloys Compd.*, 2021, **850**, 156744.
55 A. N. Carneiro Neto, E. Mamontova, A. M. P. Botas, C. D. S. Brites, R. A. S. Ferreira, J. Rouquette, Y. Guari, J. Larionova, J. Long and L. D. Carlos, Rationalizing the Thermal Response of Dual-Center Molecular Thermometers: The Example of an Eu/Tb Coordination Complex, *Adv. Opt. Mater.*, 2021, **n/a**, 2101870.

56 S. Ogo, L. T. T. Minh, T. Kikunaga, T. Ando, T. Matsumoto, T. Yatabe and K. Kato, Direct Synthesis of Hydrogen Peroxide in Water by Means of a Rh-Based Catalyst, *Organometallics*, 2020, **39**, 3731-3741.
57 S. J. Lyle and M. M. Rahman, Complexometric titration of yttrium and the lanthanons—I, *Talanta*, 1963, **10**, 1177-1182.
58 L. Krause, R. Herbst-Irmer, G. M. Sheldrick and D. Stalke, Comparison of silver and molybdenum microfocus X-ray sources for single-crystal structure determination, *J. Appl. Crystallogr.*, 2015, **48**, 3-10.
59 G. Sheldrick, SHELXT - Integrated space-group and crystal-structure determination, *Acta Crystallogr., Sect. A*, 2015, **71**, 3-8.
60 G. Sheldrick, Crystal structure refinement with SHELXL, *Acta Cryst. C.*, 2015, **71**, 3-8.
61 D. Casanova, M. Llunell, P. Alemany and S. Alvarez, The Rich Stereochemistry of Eight-Vertex Polyhedra: A Continuous Shape Measures Study, *Chem. Eur. J.*, 2005, **11**, 1479-1494.
62 J. H. Van Vleck, *The theory of electric and magnetic susceptibilities*, Clarendon Press, 1932.
63 O. Kahn, Molecular magnetism, *VCH Publishers, Inc.(USA), 1993*, 1993, 393.
64 L. Ungur and L. F. Chibotaru, Ab Initio Crystal Field for Lanthanides, *Chem. Eur. J.*, 2017, **23**, 3708-3718.
65 J. Jung, M. Atanasov and F. Neese, Ab Initio Ligand-Field Theory Analysis and Covalency Trends in Actinide and Lanthanide Free Ions and Octahedral Complexes, *Inorg. Chem.*, 2017, **56**, 8802-8816.
66 K.-X. Yu, J. G. Kragskow, Y.-S. Ding, Y.-Q. Zhai, D. Reta, N. F. Chilton and Y.-Z. Zheng, Enhancing Magnetic Hysteresis in Single-Molecule Magnets by Ligand Functionalization, *Chem*, 2020, **6**, 1777-1793.
67 M. Briganti, F. Santanni, L. Tesi, F. Totti, R. Sessoli and A. Lunghi, A Complete Ab Initio View of Orbach and Raman Spin–Lattice Relaxation in a Dysprosium Coordination Compound, *J. Am. Chem. Soc.*, 2021, **143**, 13633-13645.
68 K. Binnemans, Lanthanide-based luminescent hybrid materials, *Coord. Chem. Rev.* , 2009, **109**, 4283.
69 V. Balzani, P. Ceroni and A. Juris, *Photochemistry and photophysics: concepts, research, applications*, John Wiley & Sons, 2014.
70 J. C. G. Bunzli and C. Piguet, Taking advantage of luminescent lanthanide ions, *Chem. Soc. Rev.*, 2005, **34**, 1048-1077.
71 J. C. G. Bunzli and V. K. Pecharsky, *Handbook on the Physics and Chemistry of Rare Earths: Including Actinides*, Elsevier Science, 2016.
72 L. D. Carlos, R. A. S. Ferreira, V. de Zea Bermudez and S. J. L. Ribeiro, Lanthanide-containing light-emitting organic-inorganic hybrids: A bet on the future, *Adv. Mater.*, 2009, **21**, 509-534.
73 M. Latva, H. Takalo, V.-M. Mukkala, C. Matachescu, J. C. Rodríguez-Ubis and J. Kankare, Correlation between the lowest triplet state energy level of the ligand and lanthanide(III) luminescence quantum yield, *J. Lumin.*, 1997, **75**, 149-169.
74 A. D. Becke, Density-functional thermochemistry. III. The role of exact exchange, *J. Chem. Phys.*, 1993, **98**, 5648-5652.
75 C. Lee, W. Yang and R. G. Parr, Development of the Colle-Salvetti correlation-energy formula into a functional of the electron density, *Phys. Rev. B*, 1988, **37**, 785-789.
76 M. Dolg, H. Stoll and H. Preuss, Energy-adjusted ab initio pseudopotentials for the rare earth elements, *J. Chem. Phys.*, 1989, **90**, 1730-1734.
77 O. L. Malta, Ligand—rare-earth ion energy transfer in coordination compounds. A theoretical approach, *J. Lumin.*, 1997, **71**, 229-236.
78 W. J. C. Grant, Role of Rate Equations in the Theory of Luminescent Energy Transfer, *Phys. Rev. B*, 1971, **4**, 648-663.
79 J. C. Miller, J. S. Meek and S. J. Strickler, Heavy atom effects on the triplet lifetimes of naphthalene and phenanthrene, *J. Am. Chem. Soc.*, 1977, **99**, 8175-8179.
80 S. Tobita, M. Arakawa and I. Tanaka, The paramagnetic metal effect on the ligand localized S1 .apprx. .fwdarw. T1 intersystem crossing in the rare-earth-metal complexes with methyl salicylate, *J. Phys. Chem.*, 1985, **89**, 5649-5654.
81 L. Wang, Q. Ou, Q. Peng and Z. Shuai, Theoretical Characterizations of TADF Materials: Roles of ΔG and the Singlet–Triplet Excited States Interconversion, *J. Phys. Chem. A*, 2021, **125**, 1468-1475.
82 M. W. Mara, D. S. Tatum, A.-M. March, G. Doumy, E. G. Moore and K. N. Raymond, Energy Transfer from Antenna Ligand to Europium(III) Followed Using Ultrafast Optical and X-ray Spectroscopy, *J. Am. Chem. Soc.*, 2019, **141**, 11071-11081.
83 C. D. S. Brites, A. Millán and L. D. Carlos, in *Handbook on the Physics and Chemistry of Rare Earths*, eds. B. Jean-Claude and P. Vitalij K, Elsevier, 2016, vol. 49, pp. 339-427.
84 M. Jia, Z. Sun, M. Zhang, H. Xu and Z. Fu, What determines the performance of lanthanide-based ratiometric nanothermometers?, *Nanoscale*, 2020, **12**, 20776-20785.
85 A. N. Carneiro Neto, R. T. Moura and O. L. Malta, On the mechanisms of non-radiative energy transfer between lanthanide ions: centrosymmetric systems, *J. Lumin.*, 2019, **210**, 342-347.
86 X. Qin, J. Xu, Y. Wu and X. Liu, Energy-Transfer Editing in Lanthanide-Activated Upconversion Nanocrystals: A Toolbox for Emerging Applications, *ACS Central Science*, 2019, **5**, 29-42.
87 A. S. Souza, L. A. O. Nunes, I. G. N. Silva, F. A. M. Oliveira, L. L. da Luz, H. F. Brito, M. C. F. C. Felinto, R. A. S. Ferreira, S. A. Júnior, L. D. Carlos and O. L. Malta, Highly-sensitive Eu3+ ratiometric thermometers based on excited state absorption with predictable calibration, *Nanoscale*, 2016, **8**, 5327-5333.
88 R. T. Moura Jr, J. A. Oliveira, I. A. Santos, E. M. de Lima, L. D. Carlos, E. C. Aguiar and A. N. C. Neto, Theoretical Evidence of the Singlet Predominance in the Intramolecular Energy Transfer in Ruhemann's Purple Tb(III) Complexes, *Adv. Theory Simul.*, 2021, **4**, 2000304.
89 K. Rademaker, W. F. Krupke, R. H. Page, S. A. Payne, K. Petermann, G. Huber, A. P. Yelisseyev, L. I. Isaenko, U. N. Roy, A. Burger, K. C. Mandal and K. Nitsch, Optical properties of Nd3+- and Tb3+-doped KPb2Br5 and RbPb2Br5 with low nonradiative decay, *J. Opt. Soc. Am. B*, 2004, **21**, 2117-2129.
90 U. N. Roy, R. H. Hawrami, Y. Cui, S. Morgan, A. Burger, K. C. Mandal, C. C. Noblitt, S. A. Speakman, K. Rademaker and S. A. Payne, Tb3+-doped KPb2Br5: Low-energy phonon mid-infrared laser crystal, *Appl. Phys. Lett.*, 2005, **86**, 151911.
91 E. Kasprzycka, V. A. Trush, V. M. Amirkhanov, L. Jerzykiewicz, O. L. Malta, J. Legendziewicz and P. Gawryszewska, Contribution of Energy Transfer from the Singlet State to the Sensitization of Eu3+ and Tb3+ Luminescence by Sulfonylamidophosphates, *Chem. Eur. J.*, 2017, **23**, 1318-1330.

92 E. Kasprzycka, A. N. Carneiro Neto, V. A. Trush, L. Jerzykiewicz, V. M. Amirkhanov, O. L. Malta, J. Legendziewicz and P. Gawryszewska, How minor structural changes generate major consequences in photophysical properties of RE coordination compounds; resonance effect, LMCT state, *J. Rare Earths*, 2020, **38**, 552-563.
93 A. S. Souza, L. A. Nunes, M. C. F. C. Felinto, H. F. Brito and O. L. Malta, On the quenching of trivalent terbium luminescence by ligand low lying triplet state energy and the role of the 7F5 level: The [Tb(tta)3 (H2O)2] case, *J. Lumin.*, 2015, **167**, 167-171.
94 R. T. Moura Jr, A. N. Carneiro Neto, E. C. Aguiar, C. V. Santos-Jr, E. M. de Lima, W. M. Faustino, E. E. S. Teotonio, H. F. Brito, M. C. F. C. Felinto, R. A. S. Ferreira, L. D. Carlos, R. L. Longo and O. L. Malta, (INVITED) JOYSpectra: A web platform for luminescence of lanthanides, *Optical Materials: X*, 2021, **11**, 100080.